

Semi-Annual Report Submitted to the
National Aeronautics and Space Administration

For January - June, 1998

Contract Number: NAS5-31370
Land Surface Temperature Measurements
from EOS MODIS Data

MODIS Team Member
PRINCIPAL INVESTIGATOR

ZHENGMING WAN

P.I.'s Address:

ZHENGMING WAN
Institute for Computational Earth System Science
University of California
Santa Barbara, CA 93106-3060

phone : (805) 893-4541
Fax no: (805) 893-2578
Internet: wan@icess.ucsb.edu

Land Surface Temperature Measurements from EOS MODIS Data

Semi-Annual Report for July - December, 1997

Zhengming Wan

Abstract

We made more tests of the version 2.0 daily Level 2 and Level 3 Land-Surface Temperature (LST) code (PGE16) jointly with the MODIS Science Data Support Team (SDST). After making minor changes a few times, the PGE16 code has been successfully integrated and tested by MODIS SDST, and recently has passed the inspection at the Goddard Distributed Active Archive Center (DAAC).

We conducted a field campaign in the area of Mono Lake, California on March 10, 1998, in order to validate the MODIS LST algorithm in cold and dry conditions. Two MODIS Airborne Simulator (MAS) flights were completed during the field campaign, one before noon, and another around 10pm PST. The weather condition for the daytime flight was perfect: clear sky, the column water vapor measured by radiosonde around 0.3 cm, and wind speed less than a half meter per second. The quality of MAS data is good for both day and night flights. We analyzed the noise equivalent temperature difference ($NE\Delta T$) and the calibration accuracy of the seven MAS thermal infrared (TIR) bands, that are used in the MODIS day/night LST algorithm, with daytime MAS data over four flat homogeneous study areas: two on Grant Lake (covered with ice and snow, respectively), one on Mono Lake, and another on the snow field site where we made field measurements. $NE\Delta T$ ranges from 0.2 to 0.6°K for bands 42, 45, 46, and 48. It ranges from 0.8 to 1.1°K for bands 30-32. The day and night MAS data have been used to retrieve surface temperature and emissivities in these bands. A simple method to correct the effect of night thin cirrus has been incorporated into the day/night LST algorithm in dry atmospheric conditions. We compared the retrieved surface temperatures with those measured with TIR spectrometer, radiometers and thermistors in the snow test site, and the retrieved emissivity images with topographic map. The daytime LST values match well within 1°K. The night LST retrieved from MAS data is 3.3°K colder than those from field measurements most likely because of the effect of haze at night. The good agreement among the regional averaged surface temperatures obtained from LST values retrieved at different resolutions increased our confidence in the MODIS day/night LST algorithm.

Recent Papers Published

- Z. Wan, Y.-Z. Feng, Y. Zhang and M. D. King, "Land-surface temperature and emissivity retrieval from MODIS Airborne Simulator (MAS) data", Summaries of the Seventh JPL Airborne Earth Science Workshop, January 12-16, 1998, JPL Publication 97-21, vol. 3, pp. 57-66.
- W. Snyder and Z. Wan, "BRDF models to predict spectral reflectance and emissivity in the thermal infrared", IEEE Trans. Geosci. Remote Sensing, vol. 36, no. 1, pp. 214-225, 1998.
- W. Snyder, Z. Wan, Y. Zhang and Y.-Z. Feng, "Classification-based emissivity for the EOS/MODIS land surface temperature algorithm", Int. J. Remote Sensing, June 1998.
- X. Li and Z. Wan, "Comments on reciprocity in the directional reflectance modeling", Progress in Natural Science, vol. 8, no. 3, pp. 354-358, 1998.
- W. Snyder, Z. Wan and X. Li, "Thermodynamic constraints on reflectance reciprocity and Kirchhoff's law", Applied Optics, vol. 37, no. 16, pp. 3464-3470, 1998.

1. Status of the V2 LST Code Delivery

We have delivered two version 2.0 LST codes to the MODIS SDST in December 1997, one for PGE16 generating the daily Level 2 and Level 3 (1km and 5km) LST products, and another for the 8-day 1km Level 3 LST product. New toolkits sdptk5.2v1.00, HDF4.1r1 and mapi2.2.1 were used in the code development for this delivery. Metadata and QA (quality assurance) attributes were also implemented in the V2 code. Since then, we have made more tests for the PGE16 code jointly with SDST. We tested it with granules of MODIS simulation data in day mode or night mode only, and in both day-and-night mode. SDST made some changes in the metadata configuration file according to the requirements of the EOSDIS (Earth Observing System Data and Information System) Core System. After making minor changes a few times, the PGE16 code has been successfully integrated and tested by MODIS SDST, and recently has passed the inspection at Goddard DAAC. We are working on the establishment of a complete set of look-up tables with the MODIS PFM spectral response functions. These look-up tables will be delivered in the version 2.1 code for at-launch LST processing.

2. Field Campaign in March 1998 for the LST Validation

2.1. Test Site and Field Campaign

Because snow is the major water resource for the State of California and it is difficult to make field measurements of LST in cold regions, we have tried four field campaigns for the validation of LST algorithms in the area of Mono Lake and Mammoth Lake, California in 1994-1996, and MAS flights were requested for all except the first one. We had not obtained a complete good data set including MAS data, TIR field measurement data, and radiosonde data in a single day from these field campaigns because of weather conditions (scattered clouds over the test site) or lack of field measurement data due to changes in the MAS flight schedule.

Finally, we had a successful field campaign in this area in March 1998. For this field campaign, two weeks of MAS flight opportunity were requested. The MAS flight lines were selected in the north-south direction, covering Mono Lake, snow in the maintains and valleys, and forest areas. Details of the MAS flight lines can be found in flight numbers 98-032 and 98-033 on the web page at the NASA Ames Research Center (http://asapdata.arc.nasa.gov/ames_index.html). Five groups were interested in this field campaigns, two from the MODIS Team, one from the AirMISR team, and two groups of validation scientists. But two groups could not participate because we got the announcement of the confirmed flight

schedule only ten days before the first possible flight on March 9, 1998.

On March 9, 1998, the ER-2 Operation Office at NASA Dryden Flight Research Center and the Earth Science Division at NASA Ames conducted a test flight for the MAS instrument after its maintenance service. March 10, 1998 was a very nice day with clear-skies. The measured wind speed was less than a half meter per second and the column water vapor measured by radiosonde was around 0.3 cm. The daytime MAS flight passed the test site around 11:30 PST. The sky remained clear until early evening so we decided to conduct the night MAS flight mission on the same day. The night MAS flight passed the test area around 10pm PST. We observed some light haze moving slowly in the sky. It was more obvious in the far distant mountains. Two radiosonde balloons were launched, one for the daytime MAS flight, and another for the night MAS flight. We conducted ground measurements at a site in the snow field approximately 1 km from the crossing of Highways 395 and 120 in the east, and 70 m from Highway 120 in the north side. A reduced copy of the topographic map covering our test site and other interesting sites is shown in Fig. 1. We used one MIDAC TIR spectrometer to measure temporal TIR radiance from the snow surface. The spectrometer scanned from east to west at viewing angles 30 to -30 degree in steps of 15 degree. Six broadband radiometers (in wavelength range 10-13 μ m) were placed at 2 m above the surface to measure the snow surface temperature. Six thermistors were placed a few mm beneath the snow surface to try the contact measurement of the near-surface snow temperature. The distance between individual radiometers and thermistors was approximately 50 m. We recorded measurement data from these field instruments during day and night on portable computers and data loggers. We will analyze and compare the measurement data from MAS and field instruments in the following sections.

2.2. Quality Evaluation of the MAS Data

We received the tapes of MAS data in 1B format from NASA Ames one week after the MAS flights. We visualized the MAS images, and confirmed that the quality of the MAS data is good in general. Detailed information on the characteristics of the MAS instrument is given in a published paper [King et al., 1996]. The daytime and nighttime MAS images in bands 30, 42 and 45 are shown in Fig. 2 and Fig. 3, respectively. There are 1000 lines, 716 pixels each line in these images. Each pixel represents a spot of approximately 50 m by 50 m (more close to 45 m because the surface elevation is around 2 km in the region) on the ground. The daytime MAS images are a segment of the day flight track4 1B file, starting from the 1601th line in the 1B file. The nighttime MAS images are a segment of the night flight track4 1B

file, starting from the 1351th line in the 1B file. The band brightness temperature given in these TIR band images is calculated from the pixel radiance value calibrated by the new method [King et al., 1996], which uses the MAS relative spectral response functions and corrects the effect of the non-unit blackbody emissivity. The radiance to temperature conversion is given by the adjusted Planck function

$$I_b = B(\lambda_b, \alpha_1 T_b + \alpha_0). \quad (1)$$

where I_b is the band radiance, T_b is the band brightness temperature. The values of the central wavelength λ_b , coefficients α_1 and α_0 for band b are all given in the MAS 1B file. The color composite images based on images enhanced by the histogram equalization method in these three bands are shown in Fig. 4 and Fig. 5. Mono Lake, Highways 395 and 120, Mono Craters, forest areas are shown better in the enhanced color images. The color composite of daytime MAS images in bands 1 (peak wavelength at 470 nm), 3 (650 nm), and 7 (870 nm) is shown in Fig. 6. The black area on the top is Mono Lake, white areas are snow and white with light pink represents thin snow-cover areas. The black area (5 mm wide by 8 mm height) in the middle left is a part of Grant Lake which was covered by thin ice. The northern part of Grant Lake was covered with snow. The near infrared color film taken with 6" RC-10 (CIR) camera on the same ER-2 aircraft carrying the MAS instrument indicates that the thin ice cover on Grant Lake was in the state of melting because we can see some strips in the ice area and some small blocks of water surface in black by the edge. A portion of the image scanned from the near infrared color film, that contains the Grant Lake, is shown in Fig. 7. The two lines on the upper right corner are Highway 395.

Because day and night MAS images are needed to register together in the latitude and longitude locations of each pixels before the day/night LST algorithm is used to retrieve the land-surface temperature and emissivity. We selected six ground control points that are obvious on both day and night MAS images. We observed that some segments of Highway 395 are not shown well on the night MAS image maybe because of thin cirrus clouds. These control points are crossings and turning points on Highway 395. We used the latitude and longitude values of these group control points given in the day and night MAS 1B files to check the geolocation accuracy of the MAS 1B data. It is found that the error in the flight direction (line number) may be as large as several hundred meters. This means that if we use the geolocation data in the MAS 1B file in registration, the uncertainty in line numbers of the ground control points may be ten lines. Instead of using the latitude/longitude location given in the 1B file, we found the line and sample numbers of the ground control points in the day and night MAS images and then calculate their

correlations. The standard deviation of residual errors are 0.91 lines and 0.35 samples. Finally, we used the correlations to calculate the corresponding line and sample location of each daytime MAS pixel in the night MAS image and to interpolate the night brightness temperature value in the registered images in the seven TIR bands (bands 30-32, 42, 45, 46, and 48), that are used in the MODIS day/night LST algorithm.

In order to check the radiometric accuracy of the MAS TIR data in these seven bands, we calculated the averaged band brightness temperatures and standard deviations of the day MAS data over four flat homogeneous study areas: two on Grant Lake (covered with ice and snow, respectively), one on Mono Lake, and another on the snow field site where we made field measurements. They are labeled as areas A, B, M, and S, respectively, in Table 1. The first column is the band number, the second column is the band center λ_b used in Eq. 1, columns 3-6 are the mean and standard deviation (in the parentheses) of band brightness temperature T_b . The estimated minimum and maximum $NE\Delta T$ values are shown in the last two columns. The spatial variations of T_b in each study areas may be caused by the variations in surface temperature, surface reflectivity and emissivity, and in atmospheric temperature and water vapor profiles. The variations caused by the surface are minimized by the flatness and homogeneity of the selected study areas. Correlation analysis for study area A also rejects the assumption that the variations in T_b are caused mainly by the variations in surface temperature and emissivity. We use the T_b values of each pixels in bands 42 and 30 as independent variables and use the T_b values in other bands as dependent variables. Let us assume the atmosphere was uniform over the study area in this analysis. Because the spatial variation in surface temperature is represented in T_b of band 42, the spatial variation in surface reflectivity and emissivity is represented in T_b of band 30, we would find nearly perfect correlation of the dependent variable with the independent variables, i.e., the residual difference between the measured T_b value and the value calculated from the correlation would be very small. Our analysis indicates that it is not true for the T_b data set of study area A.

The atmospheric temperature and water vapor profiles measured by our radiosonde system in the snow field are shown in Fig. 8. The column water vapor calculated from the measured water vapor profile is 0.32 cm during the day MAS flight, 0.39 cm during the MAS night flight.

We made atmospheric radiative transfer simulations with the version 3.5 of the MODTRAN code [Berk et al., 1987] for the ice-covered Grant Lake surface (at elevation 2 km) based on the atmospheric temperature and water vapor profiles measured during the day flight because we are sure that it was a very clear-sky

day. We assume that the thin-ice surface temperature was -0.5°C and that it reflected solar radiation and downwelling atmospheric thermal radiative flux as a specular surface. The reflectivity of a specular ice surface can be calculated from the complex index of refraction for ice [Warren, 1984]. The simulated band brightness temperatures (T_b) in the seven MAS TIR bands are given in Table 2. The MAS T_b values obtained from the 1B data file are listed in column for comparison. The simulated T_b values based on the measured atmospheric profile are given in the fourth column. The simulated T_b values based on adjusted profiles (one for doubling the water vapor, another for shifting the temperature profile by 2°C) are given in the next two columns. Because we started the first radiosonde measurement at 10:58 PST, MAS flight passed the Grant Lake at 11:30 PST, it is reasonable to increase the atmospheric temperature by 2°C in the lower portion of the temperature profile. The changes due to the adjustments on column water vapor and temperature profile are shown in parentheses. Because the dry atmospheric condition, the effect of doubling the column water vapor on the band radiance at the top of the atmosphere is very small in all these seven bands. Even the maximum effect in band 42 is -0.13°C , not exceeding the possible instrument noise level in this band. Because of the dry atmosphere and the relative high surface elevation, the effect of changes in atmospheric temperature profile on T_b is moderate, less than 0.6°C in band 48 at the worst. The last column in Table 2 shows the difference between measured MAS T_b and those from the MODTRAN simulation for the temperature lifted atmospheric condition. The ice surface temperature may be not exactly at -0.5°C . But it should not be far from this value. If we accept this value, we can see that the uncertainty in the MAS TIR radiometric calibration is minimal in band 45, reasonable small in bands 30, 31, 42 and 46, but larger than 1°C in bands 33 and 48. We will show later that the ice surface temperature retrieved from the new day/night LST method is -0.78°C .

2.3. Surface Temperature and Emissivity Retrieval from MAS Data

The physics and mathematical method of the day/night LST algorithm to retrieve land-surface temperature and emissivity can be found in our published paper [Wan and Li, 1997], so we do not repeat here. We will focus on how making best retrieval from the MAS data collected for this field campaign, i.e., to find the best solution of surface emissivities in the seven bands, day and night surface temperatures, and related atmospheric terms so that we can minimized the sum of square of the radiance difference in the seven bands

$$\chi^2 = \sum_{j=1}^{14} \{w_j [L_j - L(j)]^2\} . \quad (2)$$

where w_j is the weight, L_j is the scaled band radiance observation value, $j = 1, 7$ for daytime, $j = 8, 14$ for nighttime. $L(j)$ is the scaled band radiance value that is calculated from the best solution of surface emissivities and temperatures, and related atmospheric terms.

We established look-up tables (LUT) from atmospheric radiative transfer simulations with the atmospheric temperature and water vapor profiles measured by our radiosonde system in the field. In the processing, we used the MAS relative spectral response functions measured by the Sensor Engineering Laboratory, Earth Science Division at NASA Ames in February 1998.

Because the MAS TIR bands have different $NE\Delta T$ values as shown in Table 1, we will put more weights on the TIR bands with smaller $NE\Delta T$ values and less weights on other TIR bands.

We observed in the field that during the night MAS flight the atmosphere was not as clear as in the daytime and that there were some thin cirrus and thin haze in the night sky. We can verify this by comparing the day and night T_b values averaged over the four study areas in Table 3. As Ackerman et al. (1990) found in the First ISCCP Region Experiment (FIRE), the brightness temperature difference between the 8 and 11 μm bands, $\Delta BT(8-11)$, is negative for clear regions, while for cirrus clouds it is positive. Gao and Wiscombe (1994) point out that the brightness temperature variations caused by the changes in surface emissivity should be considered in detection of thin cirrus clouds with this method. It is relative easy for us to detect thin cirrus clouds from MAS data because we have both day and night MAS data and we know that the atmosphere was very clear during the daytime MAS flight. After we compared the $\Delta BT(8-11)$ values (it is $T_b(42-45)$ from MAS bands 42 and 45 in our case), we found that $T_b(42-45)$ are increased more than 1.1 $^{\circ}\text{C}$ from the day flight time to the night flight time over these four study areas and that the $T_b(45-46)$ (difference in 11 and 12 μm bands) are increased less than half of this rate. This analysis confirmed our observation in the field that there were some thin cirrus clouds during the night MAS flight.

Because the effect of thin cirrus may be significant for the night MAS data, it is necessary to develop a special version of the day/night LST method taking into account the effect of thin cirrus in dry atmospheric conditions. As the first order of approximation, the effect of thin cirrus on the band radiance at the top of the atmospheric can be expressed as

$$L(j) = t_{cir}(j)L'(j) + [1 - t_{cir}(j)]B(T_{cir}) \quad (3)$$

where $t_{cir}(j)$ is the transmission of thin cirrus, $L'(j)$ is the band radiance before passing thin cirrus, and T_{cir} is the thin cirrus temperature. The transmission of thin cirrus can be expressed as

$$t_{cir}(j) = \exp(-A_j U_{cir}) \quad (4)$$

where A_j is the absorption coefficient in band j , U_{cir} is the absorber amount of thin cirrus.

We realize that the absorption coefficient of cirrus clouds depends on the ice particle shape, the particle size distribution and the particle index of refraction, and that the determination of the absorption coefficient is a research topic for a long time. In our simple method for the first order of cirrus correction, we just used the absorption coefficient of invisible cirrus clouds given in the MODTRAN code to calculate the band absorption coefficients in MAS bands 30-32, 42, 45, 46 and 48 (the values are 0.1360, 0.1767, 0.2175, 0.2467, 0.4794, 0.6041, and 0.6001) and set T_{cir} at 230 °K.

Because the effect of water vapor changes on the MAS brightness temperature in the seven bands is smaller than 0.13 °K as shown in Table 2 and we have the water vapor profile measured in the field campaign, we can use the measured value of daytime column water vapor instead of solving it in the day/night LST algorithm in general situations. Then we can replace the daytime column water vapor with the absorber amount of thin cirrus as one of the variables to be solved in the day/night LST algorithm. We implemented this simple procedure of thin cirrus correction and incorporated it into the day/night LST algorithm.

Because of the residual error in day/night registration, we usually make average of the MAS observations on 2 by 2 pixels before applying the day/night LST algorithm. We also tried averages on 4 by 4, 8 by 8, 16 by 16, 32 by 32 pixels. Our experience indicates that a smaller least-squares χ^2 does not necessarily give a better result for each individual solution of the day/night LST algorithm because there is noise in observations and this algorithm involves with the solution of multiple non-linear equations. But the averaged χ^2 for a large sets of solutions is a meaningful measure of the performance of the algorithm and the quality of the input data. We made a series of comparison by the use of the day/night LST algorithms with or without the thin cirrus correction for 992 lines of day and night MAS data. Only 704 pixels each line are processed in order to make the averaging on different sizes. We will say that the average on 2 by 2 pixels gives surface temperatures and emissivities at 100m resolution, similarly, average of 16 by 16 pixels

gives results at 800m resolution. The averaged χ^2 values from these two algorithms at different resolutions are shown in Table 4. From this table, we can get insights into two important features. First, the averaged χ^2 from the algorithm with thin cirrus correction is less than one half or one third of the values given by the algorithm without the thin cirrus correction at all resolutions. Second, the averaged χ^2 value reduces as the resolution gets coarser because the random noise in the MAS observations is reduced by averaging on more pixels.

The optical depth of night thin cirrus clouds in band 45 (at wavelength 11 μm) retrieved from MAS data at 200m resolution, as shown in Fig. 9, explains the reason why some segments of Highway 395 are not shown well on the night MAS image (Fig. 5). The regional mean of the retrieved cirrus optical depth is 0.045. Its maximum value is 0.308, confirming that the cirrus clouds are thin. Its minimum value is a small negative number (-0.08), suggesting that the simple cirrus correction method is not perfect and that it may be also related to the MAS instrument noise.

The day and night LST images retrieved from MAS data by the new day/night LST algorithm with thin cirrus correction at 100m resolution are shown in Fig. 10. The retrieved emissivities in bands 30, 42 and 45 at 100m resolution are shown in Fig. 11. If we place these two figures together with the reduced topographic map (Fig. 1), we can see the following features. Mono Lake had low temperature in daytime and high temperature at night, and high emissivities in all these three bands, similarly for the Inyo National Forest area. The day and night temperatures of Highway 395 are higher than its neighboring areas while its emissivities in these three bands are lower than its neighborhood. The Crater Mountain had higher temperature in daytime and lower emissivities, similarly for the island in the middle of Mono Lake and bare lands in mountains. There is no significant difference between emissivities of snow-cover areas and the neighboring forest areas, similarly for the daytime temperatures, but some snow-cover areas have much colder temperatures at night. We believe that the snow depth was larger in these snow-cover areas. We can show the above features better in contrast-enhanced color composite images. We calculate the day-night temperature from the retrieved day and night temperatures, and enhance the day-night temperature difference image with the histogram equalization method. Then we make the color composite image with the enhanced day-night temperature difference image in red, the enhanced day temperature image in green, and the enhanced night temperature image in blue. Fig. 12 shows enhanced color composite images with the day and night surface temperatures retrieved at four resolutions: 100 m on the upper left, 200 m on the

upper right, 400 m on the lower left, and 800 m on the lower right. We can see that there is no significant difference in spatial information in images at 100 m and 200 m resolutions. The spatial contrast in the image at 400m resolution is still good so that we can easily recognize Highway 395. The image at 800m resolution is good only for showing large surface targets. For climatic and hydrological studies at regional and global scales, LST is needed at much lower resolution. So it is interesting to check the accuracies of LST results retrieved at different resolutions and averaged over a same region. The Mono Lake region covered by the images in Fig. 12 is approximately 50 km by 35 km. Table 5 shows the mean LST values averaged from LST values retrieved at 5 different resolutions from 100 m to 1600 m. The maximum difference in the regional averaged surface temperatures is 0.13 °K and 0.04 °K for daytime and nighttime, respectively. It is within the noise level of the MAS TIR bands. The LST retrievals at 800m and 1600m resolutions essentially give the same result. Considering the noise in MAS data, larger effects caused by mis-registration of day and night images at higher resolutions, this is an excellent result.

2.4. Comparison with Field Measurement Data

We compared the retrieved surface temperature values at the snow field site with those from ground measurements. Table 6 gives the summary of LST values retrieved from MAS data at 100m resolution and field measurement data. The MAS viewing zenith angle at the snow site is 18 degree from the east direction. The LST value from MIDAC spectrometer is calculated from measured surface leaving radiance at view angle of 15 degree and the downwelling atmospheric radiative flux measured with sand-blasted aluminum diffuse reflective plate. The snow emissivity measured previously from a snow sample is used in the LST calculation. The uncertainties in snow emissivity and in the measured radiative flux are the major sources of errors in the LST calculation from the spectrometer data. Although the operating spectral range of the MIDAC spectrometer is from 3.5 to 13.5 μm , we only use the spectral data in the wavelength range of MAS band 45 (around 11 μm) within the atmospheric window in order to reduce the error due to these uncertainties. The spectral range of the broadband radiometer (Heimann TIR thermometer) is 10-13 μm . We made a correction of the emissivity effect on the LST value measured by the TIR thermometers. It is approximately 1.4 °C. The Heimann thermometers did not work well without heating when the ambient (instrument) temperature was below 0 °C, so we only used its measurement data during daytime. Under sunshine thermistors actually gave the air temperature rather than the snow surface temperature because they lost contact with snow particles due to snow melting. The daytime LST values

retrieved from MAS data and from field measurements match well within 1 °C. But we recognized that the LST retrieved from MAS data is for an area while the field of view of the spectrometer is only 30 cm in diameter and the field of view of the thermometers is approximately 1 m in diameter. The temporal and spatial variations in the snow surface temperature make the direct temperature comparison difficult. The night snow surface temperature retrieved from MAS data is 3.3 °C colder than the field measurements. One possible reason is the effect of thin haze during the night MAS flight.

2.5. Significance of the Results from the Field Campaign

March 10, 1998 was a golden day of the MAS data because of its clear dry sky and calm atmospheric conditions, especially for the daytime MAS flight. The ice-covered Grant Lake provided a good opportunity to evaluate the noise level and calibration accuracy of the seven MAS TIR bands. Although the size of Grant Lake (about 1 km wide and 4 km long) is not large enough for MODIS observations, it is large enough for MAS observations. In the future, once we evaluate the accuracy of MAS TIR bands with Grant Lake we can use the Mono Lake or other large targets on the ground to evaluate the accuracy of MODIS TIR bands by intercomparison of MAS and MODIS data. The day and night MAS data set from this field campaign also provides a chance to develop a simple method to correct the effect of thin cirrus clouds and to incorporate this method into the day/night LST algorithm. The good agreement among the regional averaged surface temperatures obtained from LST values retrieved at different resolutions increased our confidence in the MODIS day/night LST algorithm.

3. Anticipated Future Actions

In the second half of 1998, we will deliver V2.1 codes for the at-launch LST processing, and will establish a home page for the LST-validation field campaigns. We will process the MAS data collected over Death Valley, California in the March 1998 field campaign and compare the retrieved emissivity images with those obtained from MAS data of March 1997 in the same area.

ACKNOWLEDGEMENTS

This work was supported by EOS Program contract NAS5-31370 of the National Aeronautics and Space Administration. We wish to express our gratitude to Jeff Myers and his colleagues at NASA Ames Research Center and the ER-2 Operation Office at NASA Dryden Flight Research Center for the ER-2 flights and MAS data, to Daniel Dawson at Sierra Nevada Aquatic Research Laboratory, and Richard Martin, Death Valley National Park, for research/collecting permit for our field campaign in March 1998.

REFERENCES

- Ackerman, S. A., W. L. Smith, J. D. Spinhirne, and H. E. Revercomb, "The 27-28 October 1986 FIRE IFO Cirrus Case Study: spectral properties of cirrus clouds in the 8-12 μ m window," *Monthly Weather Review*, vol. 118, pp. 2377-2388, 1990.
- Berk, A., L. S. Bemstein, and D. C. Robertson, "MODTRAN: A moderate resolution model for LOWTRAN," Rep. AFGL-TR-87-0220, Burlington, MA: Spectral Sciences, Inc., 1987.
- Gao, B. C. and W. J. Wiscombe, "Surface-induced brightness temperature variations and their effects on detecting thin cirrus clouds using IR emission channels in the 8-12 μ m region," *J. Applied Meteor.*, vol. 33, no. 4, pp. 568-570, 1994.
- King, M. D., W. P. Menzel, P. S. Grant, J. S. Myers, G. T. Arnold, S. E. Platnick, L. E. Gumley, S. C. Tsay, C. C. Moeller, M. Fitzgerald, K. S. Brown, and F. G. Osterwisch, "Airborne scanning spectrometer for remote sensing of cloud, aerosol, water vapor and surface properties," *J. Atmos. Ocean. Technol.*, vol. 13, pp. 777-794, 1996.
- Wan, Z. and Z.-L. Li, "A physics-based algorithm for retrieving land-surface emissivity and temperature from EOS/MODIS data," *IEEE Trans. Geosci. Remote Sens.*, vol. 35, no. 4, pp. 980-996, 1997.
- Warren, S. G., "Optical constants of ice from the ultraviolet to the microwave," *Appl. Optics*, vol. 23, no. 8, pp. 1206-1225, 1984.

TABLE 1. Mean and standard deviation of band brightness temperature (T_b) in seven MAS bands over four flat homogeneous study areas in the Mono Lake field campaign on March 10, 1998.

MAS band no.	band center (μm)	T_b (δT_b)	T_b (δT_b)	T_b (δT_b)	T_b (δT_b)	estimated	
		($^{\circ}C$) area A	($^{\circ}C$) area B	($^{\circ}C$) area M	($^{\circ}C$) area S	$NEdT_{min}$	$NEdT_{max}$
30	3.745	-1.0 (1.75)	1.5 (1.29)	2.8 (1.27)	2.6 (1.41)	1.1	
31	3.905	-2.6 (1.19)	-1.4 (1.08)	1.8 (0.96)	-0.7 (1.16)	0.8	
32	4.064	-5.0 (1.41)	-4.3 (1.45)	-0.4 (1.27)	-4.1 (1.54)	1.1	
42	8.467	-3.0 (0.21)	-2.9 (0.22)	1.9 (0.34)	-2.9 (0.25)		0.2
45	10.975	-1.6 (0.25)	-1.4 (0.25)	4.0 (0.38)	-1.4 (0.30)		0.2
46	11.969	-2.8 (0.44)	-2.0 (0.51)	3.8 (0.49)	-2.3 (0.53)		0.4
48	13.274	-10.5 (0.71)	-9.8 (0.63)	-6.2 (0.71)	-10.0 (0.74)		0.6

Note: Noise estimates in the nearest bands by Univ. of Wisconsin from MAS data of Feb 08, 1997 over Lake Huron are 1.3, 0.9, 1.0, 0.13, 0.11, 0.25, and $0.58^{\circ}C$ (personal communication with Chris Moeller).

TABLE 2. Comparison between the MAS-measured T_b values over the ice-covered Grant Lake and those from MODTRAN3.5 simulations at $T_s = -0.5^{\circ}C$.

MAS band no.	band center (μm)	measured T_b (δT_b) ($^{\circ}C$)	calculated T_b (sensitivity to $\delta(cwv)$ and δT_a)			$T_{b-measured}$ minus $T_{b-calculated}$
			measured profiles $cwv=0.32cm$	$cwv=0.64cm$ no change in T_a	$T_a + 2^{\circ}C$ no change in cwv	
30	3.745	-0.95 (1.75)	-1.30	-1.33 (-0.03)	-1.21 (0.09)	0.26
31	3.905	-2.62 (1.19)	-2.03	-2.03 (0.00)	-1.91 (0.12)	-0.71
32	4.064	-4.97 (1.41)	-3.45	-3.45 (0.00)	-3.17 (0.28)	-1.80
42	8.467	-3.05 (0.21)	-2.36	-2.49 (-0.13)	-2.16 (0.20)	-0.89
45	10.975	-1.61 (0.25)	-1.65	-1.64 (0.01)	-1.60 (0.05)	-0.01
46	11.969	-2.77 (0.44)	-3.44	-3.36 (0.08)	-3.38 (0.06)	+0.61
48	13.274	-10.50 (0.71)	-12.55	-12.49 (0.06)	-11.98 (0.57)	+1.48

TABLE 3. Day and night MAS band brightness temperatures (T_{b-d} and T_{b-n}) averaged over four flat homogeneous study areas in the Mono Lake field campaign on March 10, 1998.

MAS band no.	band center (μm)	T_{b-d} (δT_{b-n}) ($^{\circ}\text{C}$) area A	T_{b-d} (δT_{b-n}) ($^{\circ}\text{C}$) area B	T_{b-d} (δT_{b-n}) ($^{\circ}\text{C}$) area M	T_{b-d} (δT_{b-n}) ($^{\circ}\text{C}$) area S
30	3.745	-1.0 (-6.0)	1.5 (-7.9)	2.8 (-0.1)	2.6 (-11.2)
31	3.905	-2.6 (-7.2)	-1.4 (-9.0)	1.8 (-1.1)	-0.7 (-12.5)
32	4.064	-5.0 (-8.4)	-4.3 (-10.1)	-0.4 (-2.8)	-4.1 (-13.8)
42	8.467	-3.0 (-8.5)	-2.9 (-10.4)	1.9 (-2.8)	-2.9 (-14.1)
45	10.975	-1.6 (-8.4)	-1.4 (-10.6)	4.0 (-1.9)	-1.4 (-15.7)
46	11.969	-2.8 (-9.6)	-2.0 (-11.7)	3.8 (-2.4)	-2.3 (-16.8)
48	13.274	-10.5 (-15.4)	-9.8 (-16.9)	-6.2 (-10.7)	-10.0 (-21.0)

TABLE 4. The averaged least-squares values of the day/night LST algorithm in the Mono Lake region (size of approximately 50km by 35km) based on MAS data of March 10, 1998.

with cirrus correction	averaged χ^2 value at resolution				
	100m	200m	400m	800m	1600m
No	0.0114	0.0082	0.0070	0.0064	0.0059
Yes	0.0052	0.0025	0.0021	0.0015	0.0017

TABLE 5. Mean LST values averaged from LST values retrieved at different resolutions in the Mono Lake region (size of approximately 50km by 35km) based on MAS data of March 10, 1998.

day/night time	mean LST (°C) averaged from values retrieved at resolution				
	100m	200m	400m	800m	1600m
day around 11:30 PST	2.47	2.51	2.53	2.59	2.60
night around 22:00 PST	-8.72	-8.72	-8.73	-8.69	-8.69

TABLE 6. The summary of LST values retrieved from MAS data and field measurement data over the snow field (study area S) near Mono Lake, March 10, 1998.

time	Ts (MAS)	Ts (MIDAC spectrometer)	Ts (thermometers)	Ts (thermistors)
11:28 PST	-0.8	-1.1	-0.6	3.0*
21:58 PST	-10.7	-7.4	**	-7.0

Note:

* Under sunshine thermistors gave the air temperature rather than the snow surface temperature because they lost contact with snow particles due to snow melting.

** The Heimann thermometer did not work well without heating when the ambient (instrument) temperature was below 0 °C.

Figure 2. Brightness temperatures (K) in daytime MAS bands 30 (A), 42 (B) and 45 (C),
March 10, 1986.

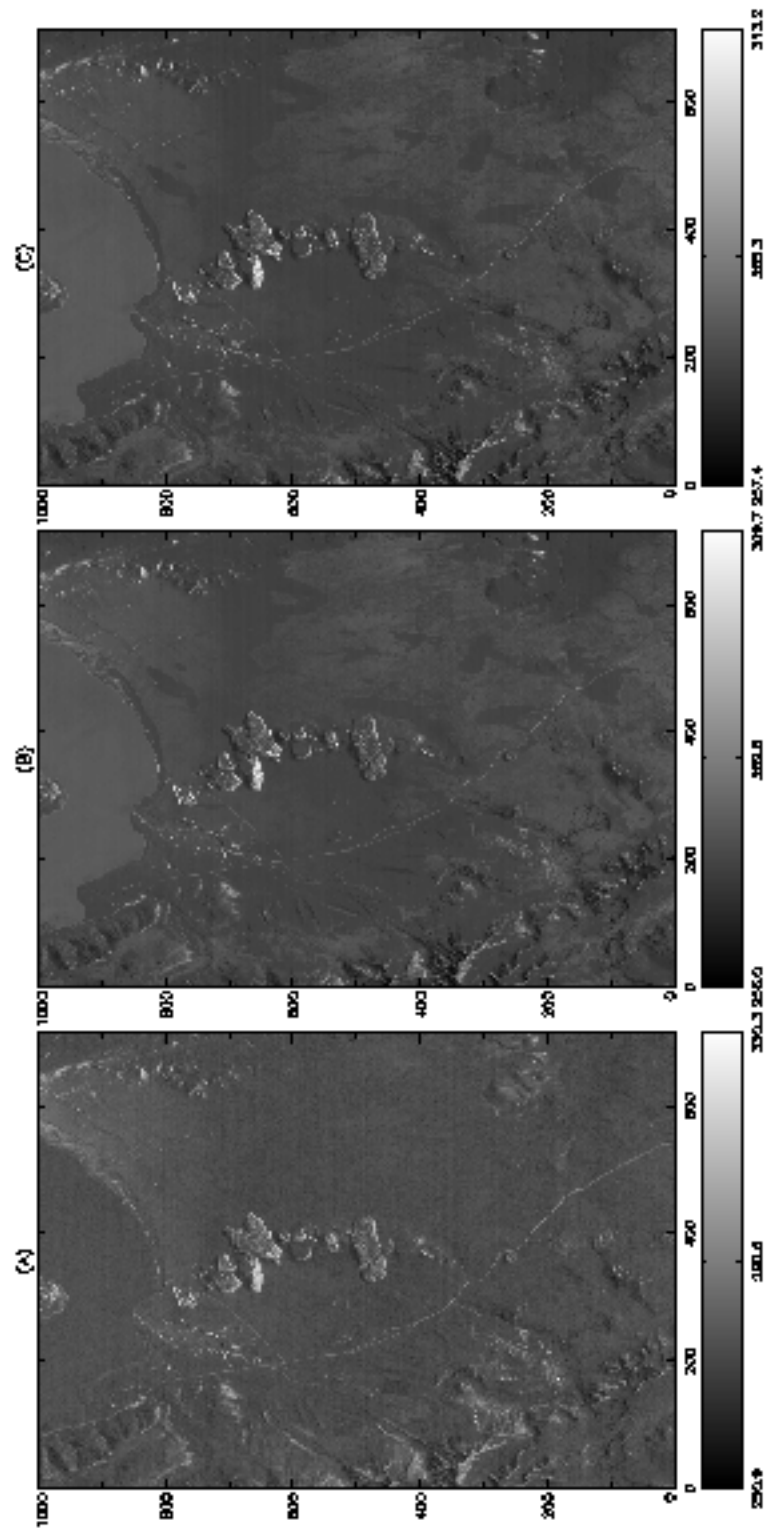
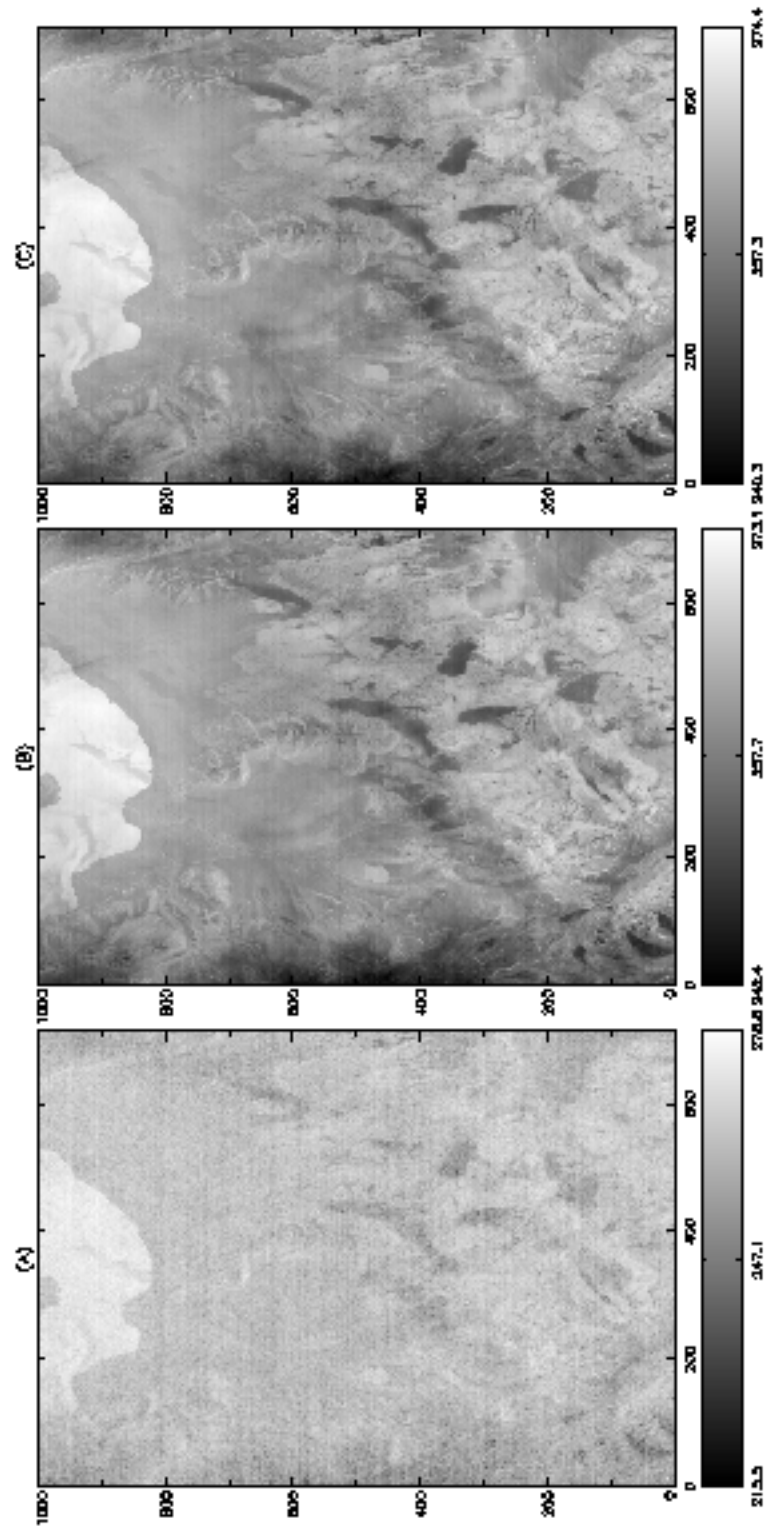
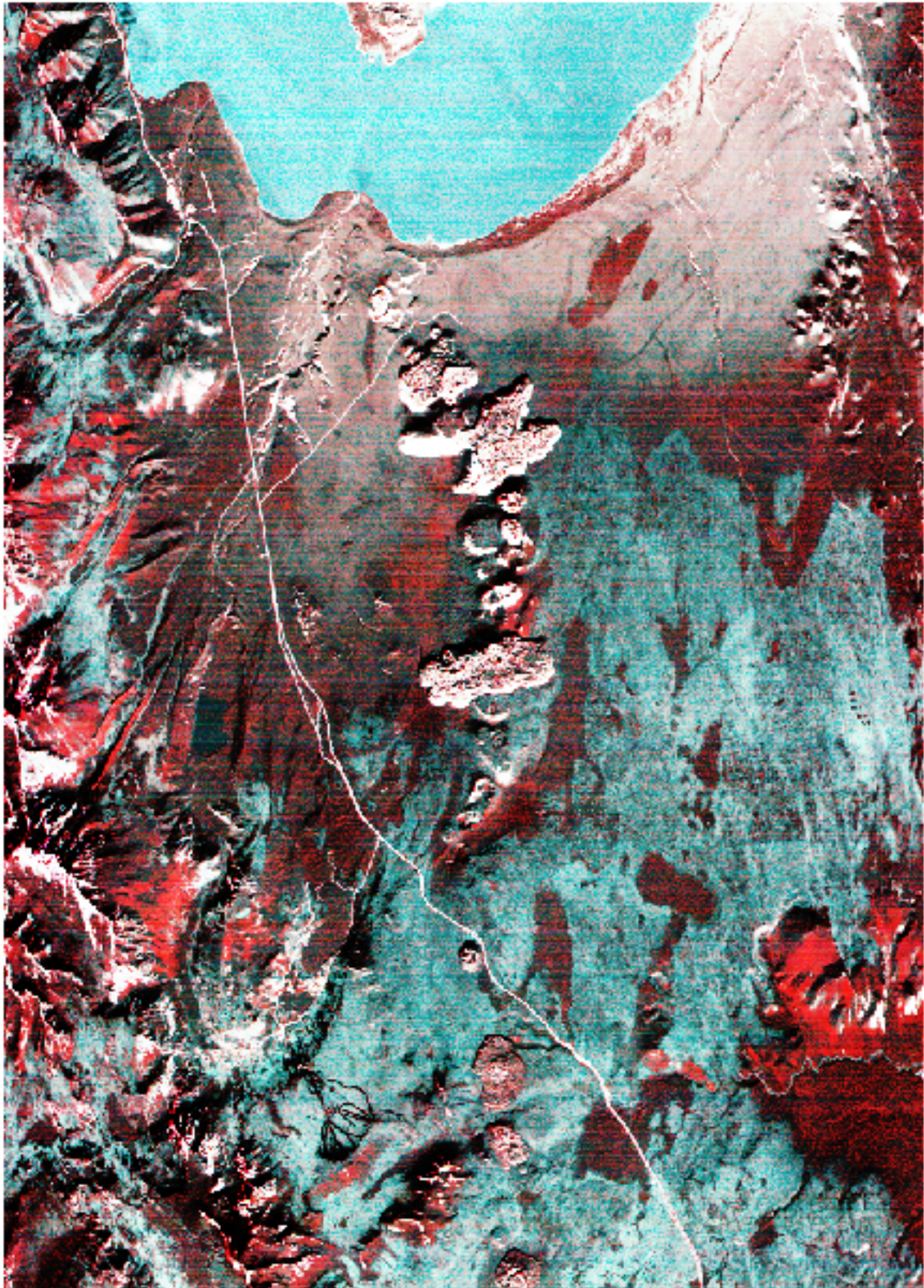


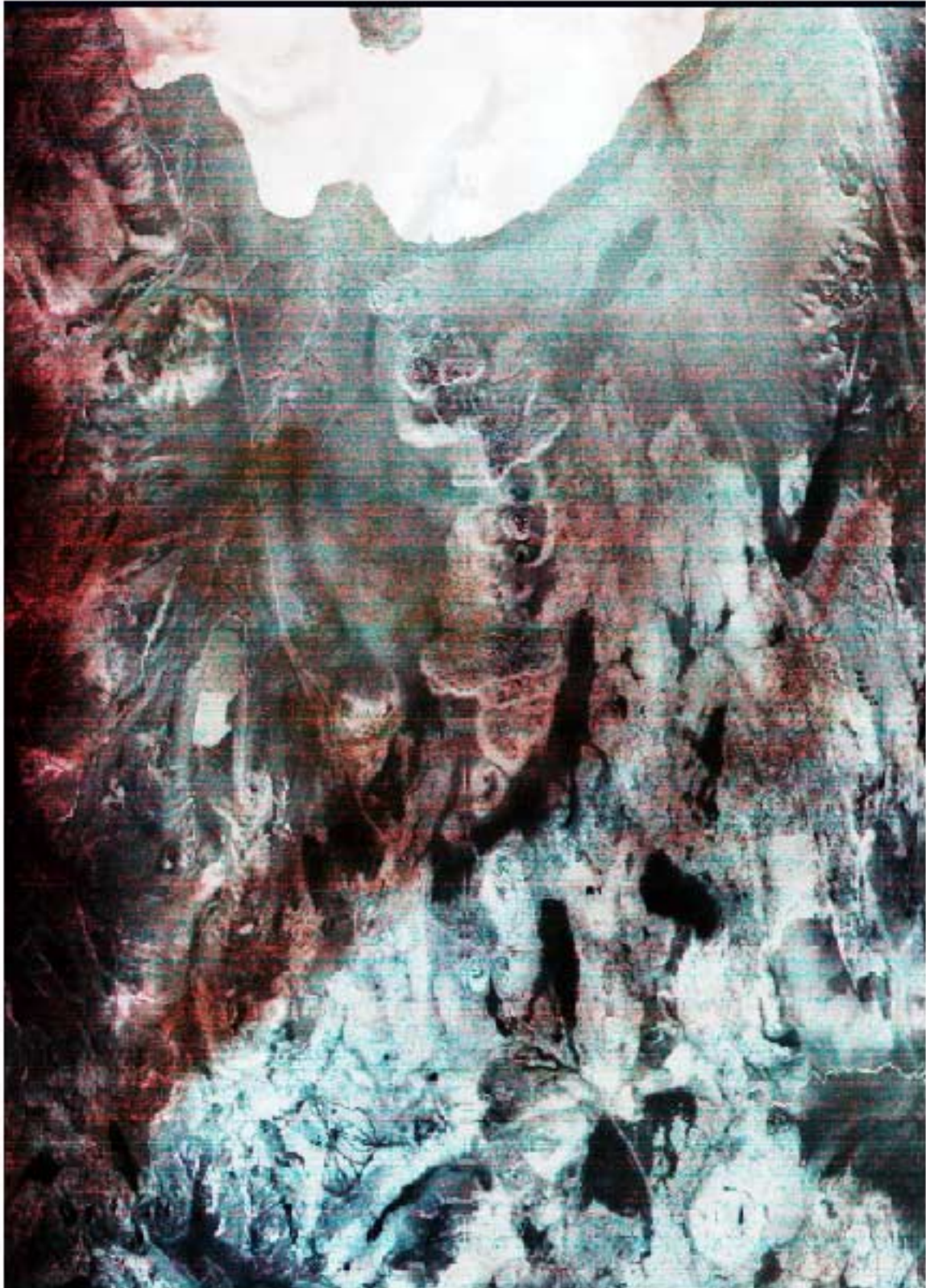
Figure 3. Brightness temperatures (K) in nighttime MAS bands 30 (A), 42 (B) and 45 (C),
March 10, 1986.



Color composite of NAS bands 30, 42 and 45 images, around 11:30PS^m, March 10, 1996



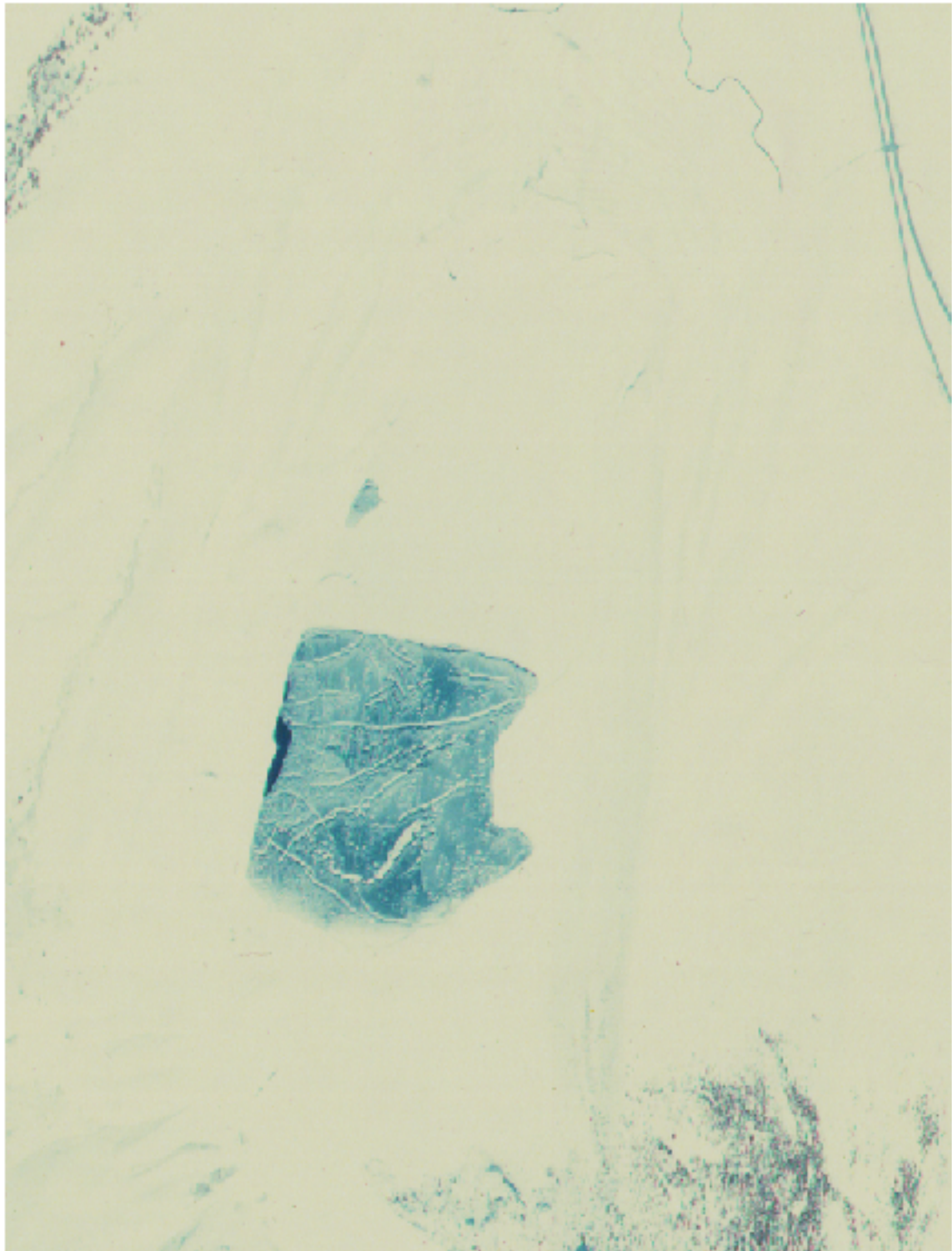
Color composite of MAS bands 30, 42 and 45 images, around 22:00PST, March 10, 1998



Color composite of MAS bands 1, 3 and 7 images, around 11:30PST, March 10, 1996



Fig. 7, Ice covered Grant Lake seen from near infrared film, March 10, 1998.



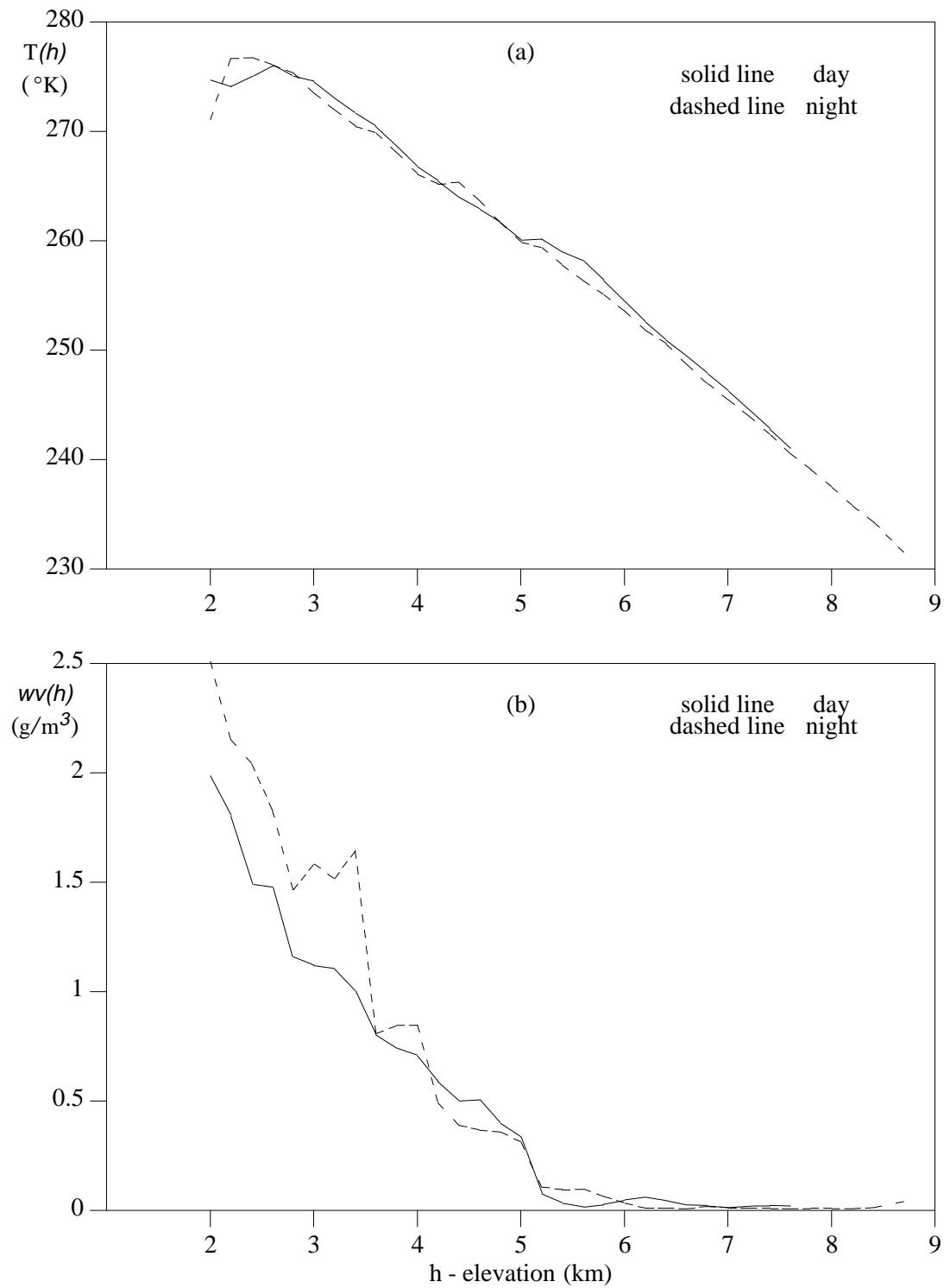


Fig. 8, Atmospheric temperature (a) and water vapor (b) profiles near Mono Lake, March 10, 1998.

Fig. 9, Optical depth of night thin cirrus retrieved from MAS data,
Mono Lake area, March 10, 1998.

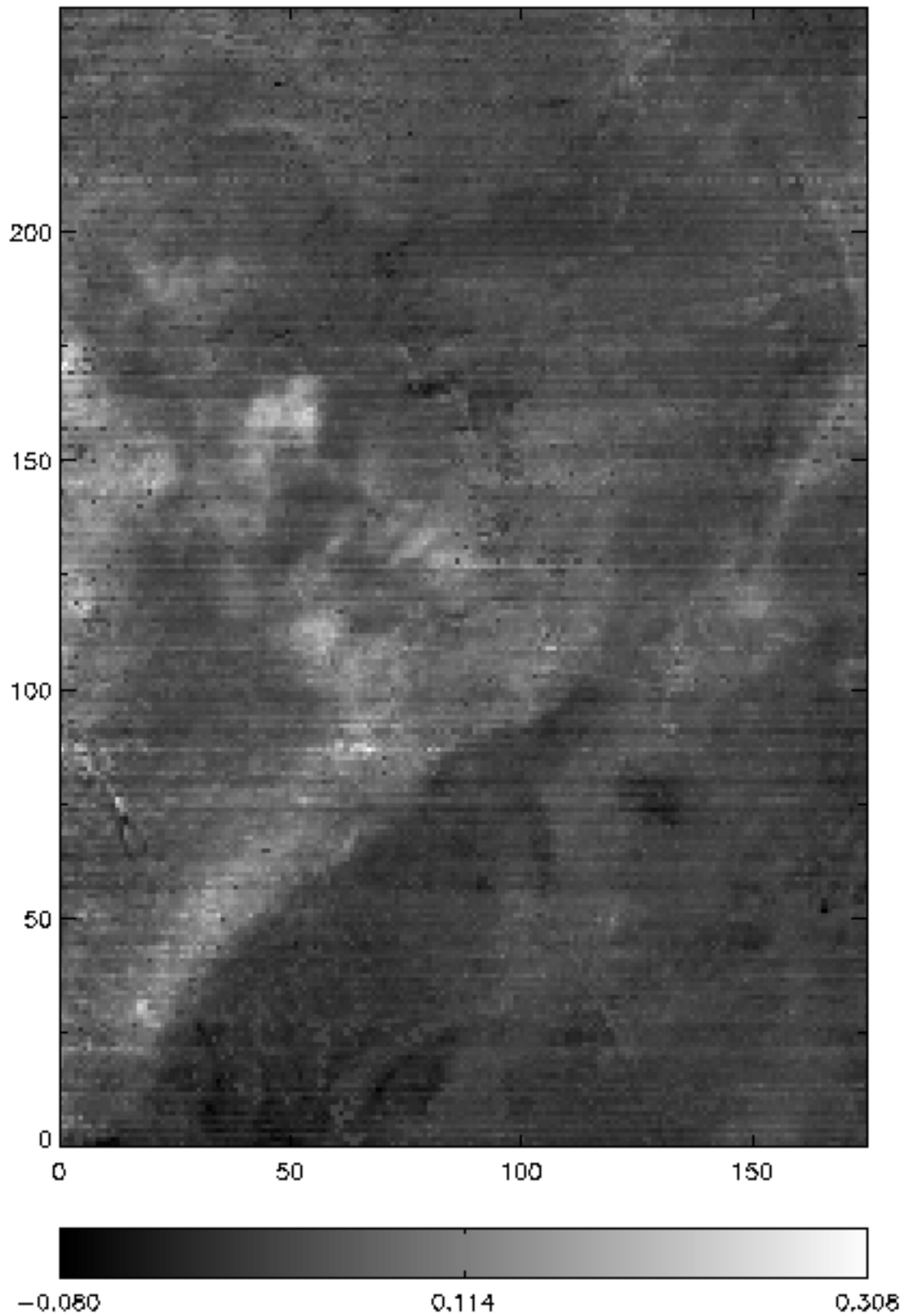


Fig. 10, Day (A) and Night (B) LST (in unit K) images retrieved from MAS data at 100m resolution, Mono Lake area, March 10, 1988.

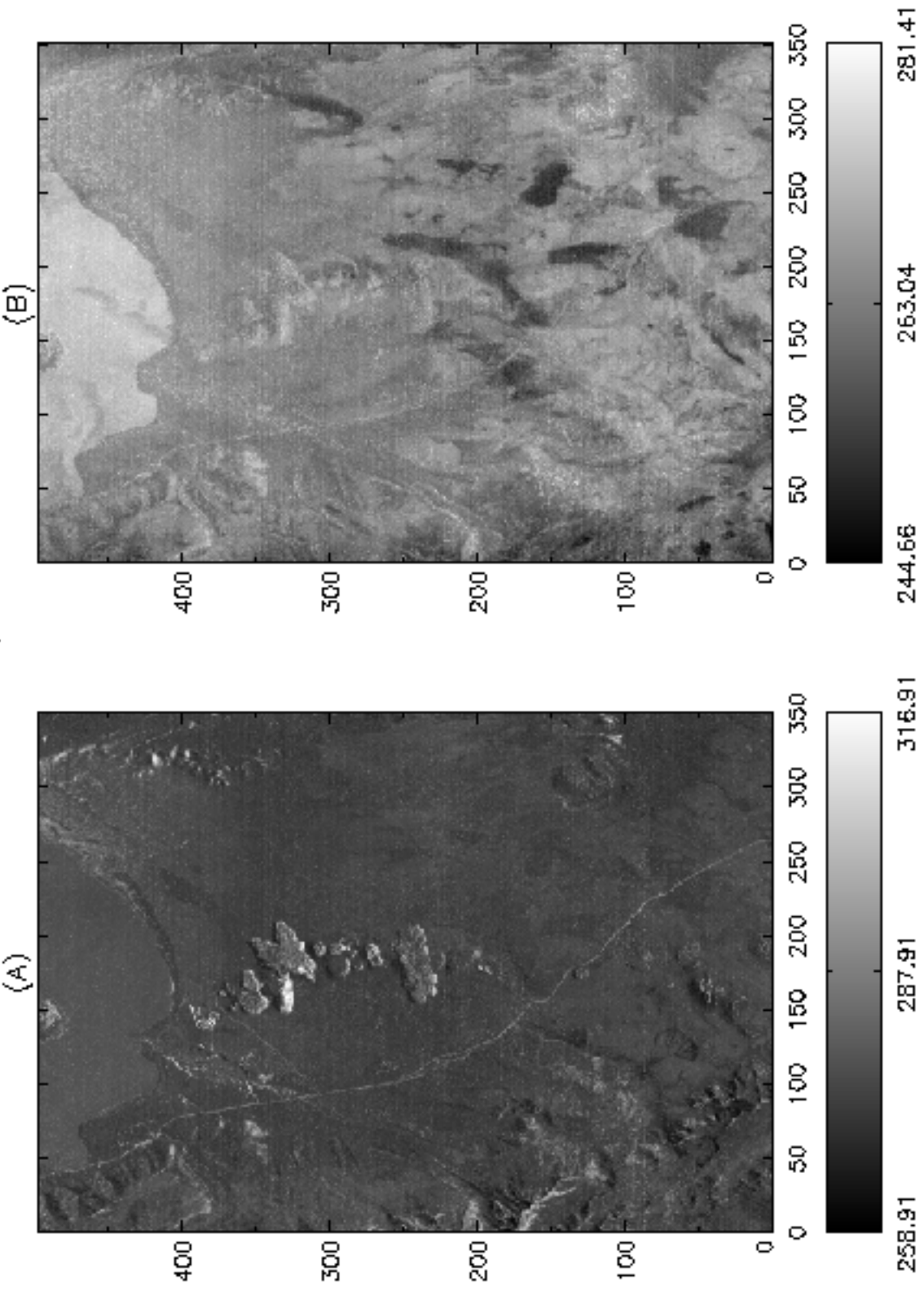


Fig. 11, Emissivities retrieved from MAS data in bands 30 (A), 42 (B) and 45 (C),

Mono Lake area, March 10, 1998.

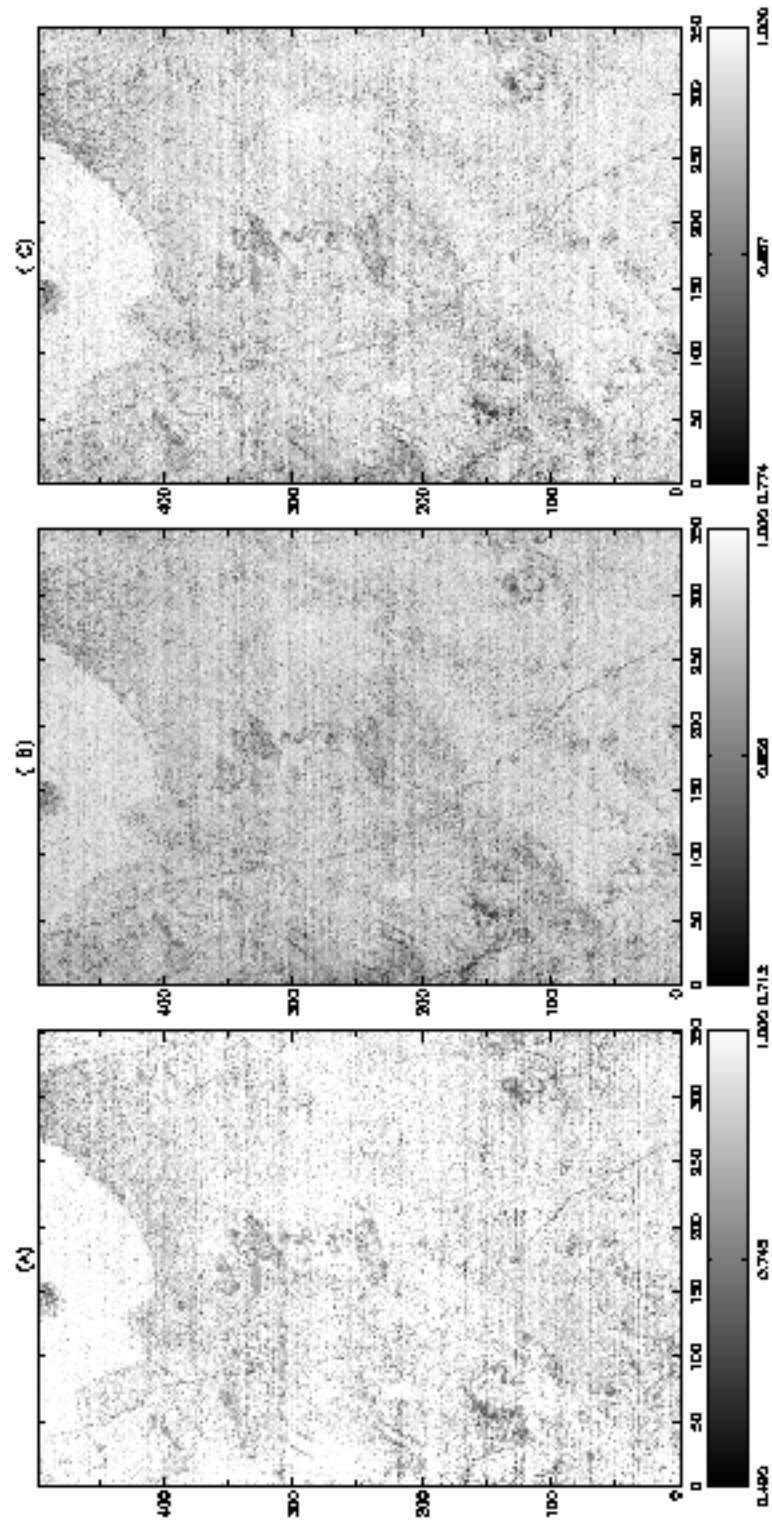


Fig. 12. Color composite of day-night difference, day and night LST images at different resolutions.

